Proc. Int. Symp. „Brittle Matrix Composites 7"
A.M. Brandt, V.C. Li and I. H. Marshall, eds.
Warsaw, October 13-15, 2003
ZTUREK RSI and Woodhead Publ., Warsaw 2003

DRYING SHRINKAGE AND CRACK WIDTH OF ENGINEERED CEMENTITIOUS COMPOSITES (ECC)

Martin B. WEIMANN and Victor C. LI

The University of Michigan, Ann Arbor, MI, U.S.A.
Advanced Civil Engineering Materials Research Laboratory
Department of Civil and Environmental Engineering

ABSTRACT

Drying shrinkage of an engineered cementitious composites (ECC) leads to eigenstress in the composite when restrained. If the eigenstress is higher than the tensile strength of the composite, crack formation will occur. Due to the engineered design of the composite the crack width is found to be less than 50μm, regardless of the specimen dimensions. From a durability point of view the composite can be considered as an effectively uncracked material. A physical model for the drying shrinkage deformation will be described. It will be demonstrated that at 50% relative humidity or below, the use of a Portland cement with a low alkali content for the ECC matrix reduces the drying shrinkage deformation and the crack width in comparison to an ECC with a normal alkali content cement matrix.

Keywords: drying shrinkage, crack, disjoining pressure, durability, ECC, low alkali cement

INTRODUCTION

Improvement of the durability of cementitious composites is from an economical and ecological point of view an important issue. An improvement of the durability can be reached with a material which shows a small crack width due to restrained drying shrinkage deformation. In order to achieve this goal it is useful to understand the intrinsic causes of macroscopic drying shrinkage.

Moisture exchange of capillary porous cement paste with the environment causes macroscopic deformations of cementitious composites. The microstructure of capillary porous cement paste consists of colloidal CSH-gel particles with at least one dimension of the particles in the range between 1nm and 1μm [1]. Different deformation mechanisms operate at this microstructure level depending on the relative humidity (RH). In this paper, we approach the study of drying shrinkage from this microscopic viewpoint.

Restrained drying shrinkage deformation of cementitious composites leads to an eigenstress in the material that can cause cracks, if this eigenstress is higher than the tensile strength of the material. In normal concrete or fiber reinforced concrete, the width of shrinkage cracks will depend on the amount of shrinkage and the dimensions of the specimen. The crack width under restrained drying shrinkage of Engineered Cementitious Composite (ECC) investigated here is a material property. This is an outcome of the unique tensile response of ECC. ECC is micromechanically designed [2] with a strain capacity more than 100 times higher than that of a normal concrete. As long as the shrinkage strain remains below the tensile strain capacity, the crack width is a material property independent of the specimen size and shape.

A reduction of the drying shrinkage deformation of ECC should lower the crack width. The use of a low alkali content Portland cement (LA-cement) reduces the drying shrinkage compared to a normal alkali content Portland cement (NA-cement) at 50% RH or below. Therefore ECC made with a LA-cement should show a lower crack width compared to ECC made with a NA-cement, at 50% RH or below.

The objective of this research is to establish crack width as a material property for ECC under restrained drying condition. It will also be shown that the already small crack width of ECC can be further reduced by the use of LA-cement, at least within a certain humidity range. A clarification of the underlying physical mechanisms of this macroscopic drying shrinkage control of ECC from the microstructural point of view is also part of this research.

In the following we will first discuss the physical mechanisms of drying shrinkage, followed by a description of the investigated materials and experiments on free and restrained drying shrinkage. The experimental results and a discussion of them are then presented. Conclusions are drawn in the last section.

REVIEW OF THE PHYSICAL MECHANISMS OF DRYING SHRINKAGE

Drying shrinkage in a cementitious material can be attributed to changes in a) surface energy of CSH-gel particles b) disjoining pressure between surfaces of CSH-gel particles, and c) capillary under-pressure [3]. The disjoining pressure defines the force of interaction per unit area of bodies that are separated by a thin parallel interlayer [4], and is a superposition of three forces. These forces are a) an attractive van der Waals force b) a repulsive electrostatic force and c) a repulsive steric force. The steric force may be altered by the introduction of polymers which will not be the focus in this paper. The electrostatic force is influenced by the charge composition of the pore solution of the cementitious composite. The importance of the three mechanisms of drying shrinkage varies with the relative humidity.

Drying shrinkage for 50% < RH < 100% is caused by an attractive capillary under-pressure which acts simultaneously with a repulsive disjoining pressure [3]. The capillary under-pressure leads to a reduction in the pore dimensions of the composite which causes a macroscopic shrinkage deformation. The Laplace equation [5] describes the under-pressure as a function of the pore radius. The charged surfaces of CSH-gel particles do not coalesce because of the disjoining pressure between the particles. The repulsive disjoining pressure is caused by an electrostatic force between the surfaces of particles which are surrounded by electric charges from the pore solution and by structured water [3]. Structured water is caused by dipole interaction of the water molecules with charged surfaces. The attractive capillary under-pressure acts only in pores which are water saturated. The radius of pores which are empty due to drying depends on the relative humidity. Kelvin's equation [5] describes the relationship between the radius of the largest water saturated pore as a function of RH.

Drying shrinkage for RH < 50% can be described in terms of an attractive capillary under-pressure and an attractive van der Waals force in addition to the repulsive part of the disjoining pressure. According to Kelvin's equation, evaporation of water in pores with a radius smaller than 1.6nm occurs when RH < 50%. It was shown that the smallest pore radius in cement paste is 1nm [6]. (The pore size in ECC has been confirmed to be in the same range as cement paste by mercury intrusion porosimetry measurements.) This means that according to Kelvin's equation all pores with a radius of 1nm are empty at 40% RH. The opposite surfaces of CSH-gel particles can coalesce when the relative humidity reaches 40% due to the

additional attractive van der Waals force which acts between the surfaces. At 40% RH, only adsorbed water on the surfaces of the particles is left. The attractive capillary under-pressure and van der Waals force are no longer responsible for drying shrinkage of RH<40%.

Drying shrinkage for RH < 40% is due to a change of surface energy of CSH-gel particles. Evaporation of adsorbed water from surfaces leads to a compression of the particles resulting in a macroscopic shrinkage deformation. The change of the surface energy can be correlated to shrinkage deformation from 40% RH to the dry state (0% RH).

The Munich model [6,7] describes hygral deformation as a result of the change in surface energy of CSH-gel particles and disjoining pressure between surfaces of CSH-gel particles in cement paste. In the following we focus on hygral deformation instead of drying shrinkage in order to be able to explain the influence of different pore solutions on the micromechanisms of deformations at changing relative humidity.

The concept of hygral deformation can be described as follows. CSH-gel particles in the dry state are under compression due to their surface tension and are held together by chemical and van der Waals bonds. Water adsorption on particles surfaces leads to an expansion of the particles due to surface energy change. For RH > 40% an additional repulsive disjoining pressure act on opposite CSH-gel surfaces which are coalesced due to van der Waals bonds. A release of van der Waals bonds leads to an additional swelling of the cement paste which is superimposed with the swelling of the CSH-gel particles due to surface energy change. The swelling of the cement paste due to moisture uptake causes an expansion of the cementitious composites which can be interpreted as a hygral deformation of the composite. The hygral deformation at a given RH can be computed from the difference between the steady state drying shrinkage value of the dry state and the steady state drying shrinkage value at that RH.

The Munich model is adopted here to describe the hygral deformation of ECC. The hygral deformation at 0% < RH < 40% is caused by a change of the surface energy $\Delta\gamma$ of CSH-gel particles [3]. Bangham [8] describes the hygral deformation $\varepsilon_{hyg,Surface}$ as a function $\Delta\gamma$:

$$\varepsilon_{hyg,Surface}(RH) = \lambda \cdot \Delta\gamma(RH) \tag{1}$$

The proportionality constant λ was introduced by Hiller [9] for porous materials. λ is a function of the modulus of elasticity, the specific surface area of the porous material, and the density of the nonporous CSH-gel. $\Delta\gamma$ can be calculated from experimentally determined volume of adsorbed water V at different RH [10,11,12]:

$$\Delta\gamma(RH) = -\frac{R \cdot T}{M \cdot A}\int_0^P \frac{V(RH)}{P(RH)}dP \tag{2}$$

Here R = universal gas constant, T = absolute temperature, M = mol volume of water, A = specific surface area and P = water vapor partial pressure which depends on RH. $RH = 100 \cdot P/P_s$ where P_s = saturated water vapor partial pressure. Equation 2 is not valid for water saturated pores because in these pores thermodynamic equilibrium is not attained [10]. Therefore $\Delta\gamma$ is not significant for RH > 40%. For RH > 40%, a hygral deformation caused by the disjoining pressure is superimposed onto that due to $\Delta\gamma$. The total hygral deformation is

$$\varepsilon_{hyg,Total}(RH) = \varepsilon_{hyg,Surface}(RH) + \varepsilon_{hyg,Disjoining-Pressure}(RH_{>40}) \tag{3}$$

Equation 3 describes the total hygral deformation of cementitious materials for relative humidity's from the dry state (0% RH) to 100%.

INFLUENCE OF LA-CEMENT ON DRYING SHRINKAGE

In the previous section we noted that the repulsive electrostatic force of the disjoining pressure is influenced by the charge composition of the pore solution. According to the DLVO-theory [13] the disjoining pressure depends on the ionic strength of the pore solution and on the surface charge of the colloidal particles. Beltzung et al. [3] investigated the influence of different pore solutions on drying shrinkage of concrete. The DLVO-theory can explain the lower drying shrinkage in a cementitious material made with a LA-cement compared to one with a NA-cement. A cementitious composite has a saturated pore solution of Calciumhydroxid [3]. The amount of divalent ions like Ca^{2+} dominates the repulsive potential of a double layer compared to monovalent ions [13]. A reduction in the amount of the monovalent alkalis Na^+ and K^+ leads to an increase of the solubility of Ca^{2+} [3], resulting in a lower repulsive double layer potential. The attractive van der Waals potential is insensitive to the ionic composition of the pore solution [13]. Figure 1a shows the repulsive double layer and the attractive van der Waals potentials. A lower repulsive double layer potential during the hydration process at 100% RH leads to a smaller equilibrium distance between the CSH-gel colloids (Fig. 1b). The smaller distance between the gel colloids in a LA-cement will result in a lower macroscopic shrinkage deformation when drying occurs.

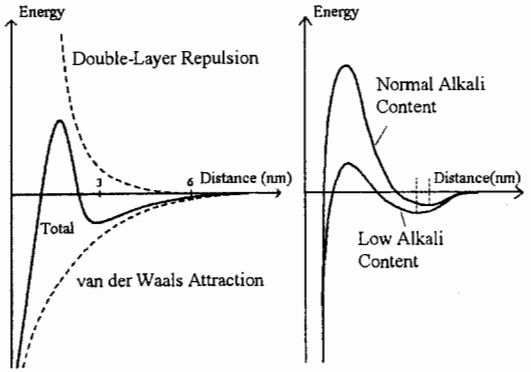

Figure. 1: Schematic illustration of total interaction energy as a function of inter-particle distance, adapted from [13] (a) by summing the double-layer repulsion potential and the van der Waals attraction potential and (b) for normal and low alkali content cements at RH 100%

EXPERIMENTS

In this research we will investigate an ECC with a normal alkali content (0.9M.-%) Portland cement and an ECC with a low alkali content (0.6M-%) Portland cement. These ECCs are reinforced with 2% by volume of PVA (PolyVinyl Alcohol) fibers. An ECC-Matrix composition with normal alkali content and without fibers will also be investigated. A small amount of **H**ydroxy**P**ropyl-**M**ethyl**C**ellulose (HPMC) was added to the ECC-Matrix composition to prevent segregation. Normal concrete is included in these experiments as a control. The mix compositions of the investigated materials are shown in Table 1.

Using a uniaxial direct tension test [14], the tensile stress-strain curves of ECC and concrete were determined. The objective of this test in combination with the free drying shrinkage test (described below) is to show that the tensile strain capacity of ECC is higher than the drying

shrinkage deformation. This means that the crack width of ECC under restrained drying shrinkage is a material property. The drying shrinkage deformation of concrete is much higher than the tensile strain capacity of concrete implying that the crack width depends on the specimen size and geometry in the case of concrete.

Table 1: Mix compositions of the investigated materials (SP = superplasticizer)

	Aggregates [kg/m^3]	Cement [kg/m^3]	Water [kg/m^3]	Fly Ash [kg/m^3]	SP [kg/m^3]	PVA-Fiber [kg/m^3]
ECC (0.9M.-%)	max. size < 150µm 467	583	298	700	17.5	26
ECC (0.6M.-%)	max. size < 150µm 467	low alkali 583	298	700	17.5	26
ECC-Matrix	max. size < 150µm 477	595	304	714	17.9 +HPMC	-
Concrete	max. size < 25mm 1728	432	192	-	-	-

Free drying shrinkage measurements were made for all four materials as a function of drying time and RH. Drying shrinkage measurements, with setup shown in Fig. 2a, were conducted based on ASTM C157/C157-99 and ASTM C596-01 [15] standards. These measurements clarify the differences in drying shrinkage behavior of the different mixes. In addition, the water mass loss per volume of the specimens was determined in order to calculate the volume content of moisture V, needed to calculate the change of the surface energy at different RH.

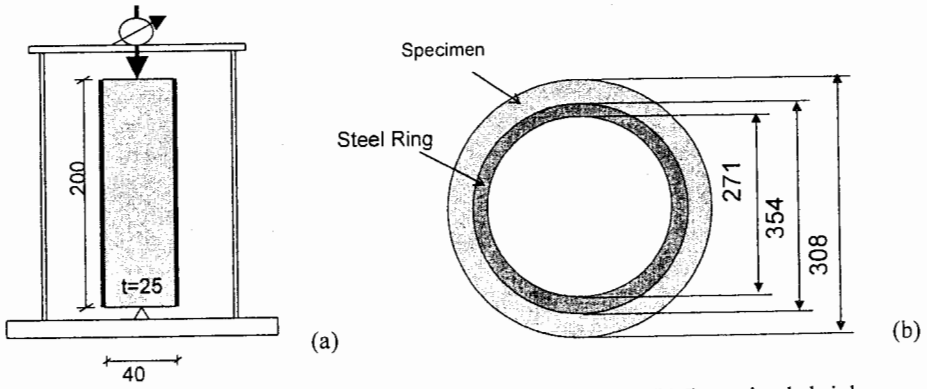

Figure 2: Experimental set up: (a) Free drying shrinkage test and (b) Restrained shrinkage ring test. Dimensions in mm.

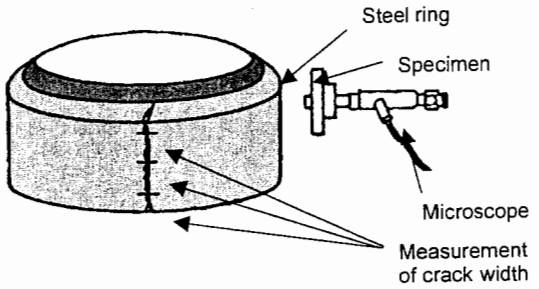

Figure 3: Ring test for determination of the crack width

Fourteen specimens for each mix were cast and demoulded after one day. After two days of storage at RH = 100% two specimens of each mix were stored in RH= 93%, 85%, 75%, 66%, 33%, 12% and 0%, obtained using oversaturated salt solutions in different desiccators [16,17]. The drying shrinkage deformation and mass loss were measured as a function of drying time until hygral equilibrium was reached. The length change was measured with an accuracy of 1μm. The mass loss was measured with an accuracy of 1mg. After all specimens had reached hygral equilibrium the specimens stored at 0% RH were dried in an oven at 105C until the mass is constant. After removing from the oven the specimens were allowed to cool down to room temperature in order to measure the hygral length change due to moisture loss. When the specimens reached thermal equilibrium with room temperature the length change and mass loss were determined and considered as values at RH = 0%.

In order to investigate the number and width of cracks, the restrained shrinkage ring test [18] was adopted (Fig. 2b). Two specimens of each mix were cast. During casting a thin plastic foil covered cardboard paper cylinder was used as an outer mold which was removed three days after casting. Subsequently, the specimens were exposed to RH = 50%. Drying of the specimen leads to an internal radial pressure in the specimen resulting from the restraint of the hygral deformation by the steel ring. For the dimensions of these specimens, it can be shown that the specimens were subject to an approximately uniaxial tensile stress state during restrained shrinkage. Figure 3 illustrates the measurement of the crack width, determined as an average value for each crack at three different locations as a function of the drying time.

RESULTS & DISCUSSIONS

Figure 4 shows the uniaxial tensile stress-strain curve and the crack width for ECC (0.9M.-%). For comparison a typical stress-strain curve of a concrete taken from the literature [19] is included. The strain values of the concrete have been expanded to show the curve more clearly. The crack width in the ECC was obtained by monitoring the opening of one of the many multiple cracks as the specimen strain increased. The crack width increases with strain up to about 1% and then stabilizes at a steady state value of about 60μm until fracture localization at ε=5.2%.

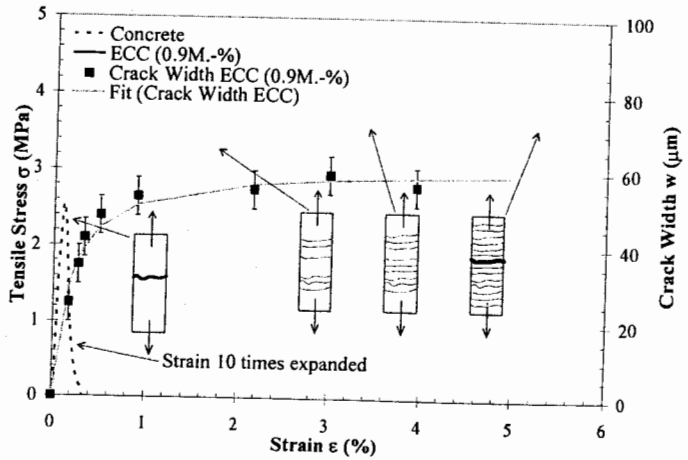

Figure 4: Tensile stress-strain curve of ECC (0.9M.-%) and concrete. The crack width as a function of tensile strain is also shown for the ECC

Figure 5 shows the calculated change of surface energy according to Eq. 2 for the investigated materials as a function of the relative humidity using the moisture content per volume for the investigated materials measured at 0%, 12% and 33% RH. The dotted lines in Fig. 5 are logarithmic fits to the change of surfaces energy for different RH in the form of

$$\Delta\gamma = A \cdot \ln(RH) + B \tag{4}$$

From the experimental data Δγ, the values of A and B are determined for each material and reported in Table 2.

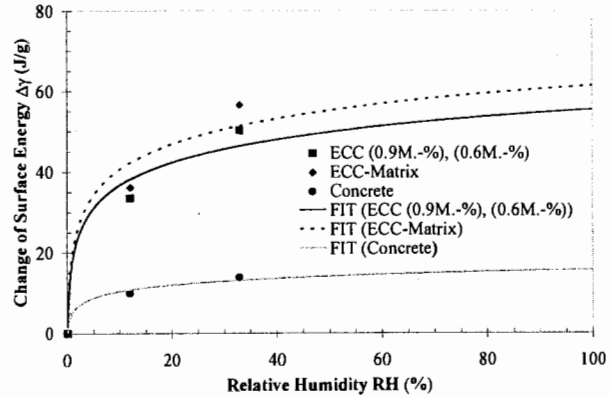

Figure 5: Experimental data and theoretical fits of change of surface energy as a function of the relative humidity for the investigated materials

Figure 6 plots the hygral deformation of the investigated materials dried to different RH's, calculated from the drying shrinkage data as the difference between the steady state drying shrinkage value in the dry state (0% RH) and the steady state drying shrinkage value at specific RH's. At 100% RH ECC (0.6M.-%) shows a lower hygral deformation due to the lower equilibrium distance between CSH-gel particles (Fig. 1) produced with LA-cement compared to NA-cement. The theoretical hygral deformation curves to be discussed in a later section are also shown in this figure. The measured crack width w as a function of the drying time is shown in Fig. 7. The specimens were exposed to RH=50%.

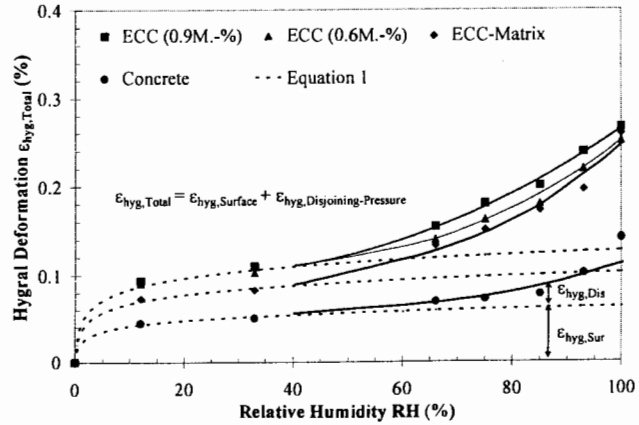

Figure 6: Experimental data and theoretical curves of hygral deformation as a function of the relative humidity for the investigated materials

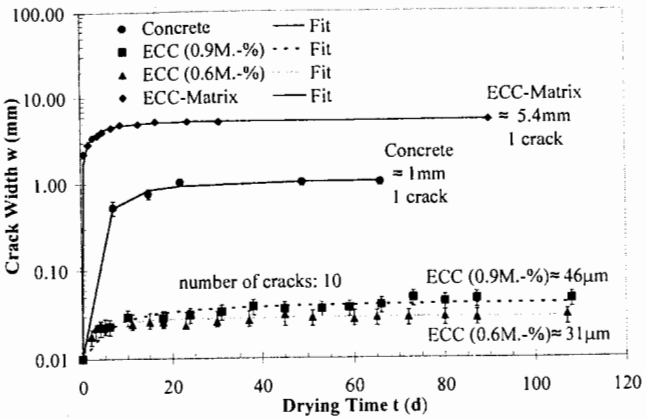

Figure 7: Crack width development as a function of drying time (at RH=50%)

The hygral deformation for the investigated cementitious materials can be described by using the Munich model originally developed for cement paste [6,7]. The expansion of CSH-gel particles is caused by a change of the surface energy of CSH-gel particles and for RH > 40%, due to an additional disjoining pressure between the surfaces of CSH-gel particles. The Munich model originally developed for porous building materials such as brick and concrete [20] is here shown to be applicable to describing the hygral deformation of ECCs.

Using Eq. 1 and 3, the total hygral deformation of the investigated materials can be rewritten in the following form:

$$\varepsilon_{hyg,Total} = \lambda \cdot (A \cdot \ln(RH) + B) + c \cdot (h - h_0)^2 + d \cdot (h - h_0) \qquad (5)$$

where c, d are empirical parameters and h, h_o are relative humidity's. The first term is from Eq. 1 and 4. The second and third term represent a second order polynominal fit to the RH dependence of $\varepsilon_{hyg,Disjoining-Pressure}$ [20]. Equation 5 is valid for $h \geq h_0$ with h_o=40. The parametric values λ, c and d for the investigated materials shown in Table 2 were obtained by fitting Eq. 5 to the total hygral deformation data reported in Fig. 6. The parametric values of λ are on the same order of magnitude as concrete reported in the literature [20].

Table 2: Parametric values of the investigated materials

	A [J/g]	B[J/g]	λ [g/J] x10^{-3}	c [-] x 10^{-5}	d [-] x 10^{-4}
ECC (0.9M.-%)	8.2	17.9	2.3	2.0	+7.1
ECC (0.6M.-%)	8.2	17.9	2.3	3.9	-2.8
ECC-Matrix	9.1	19.8	1.6	4.2	-1.1
Concrete	2.3	5.1	4.0	1.9	-3.0

The average crack width (Fig. 7) in the ECC is almost 20 times smaller compared to the crack width in concrete. A cracked concrete with a crack width smaller than 50μm has been shown to have the same permeability as an uncracked material [21]. From a durability point of view the ECC can be considered an effectively uncracked material.

As can be observed in Fig. 6, the typical drying shrinkage deformations of ECC are lower than 0.3%, so that even a small reduction of the tensile strain has a great influence of the crack width (Fig. 4). This is the reason why an ECC made with a LA-cement shows a lower

crack width compared to an ECC produced with a NA-cement. Figure 7 shows that the ECC (0.6M.-%) has a crack width of 31μm compare to 46μm for ECC (0.9M.-%).

The ECC-Matrix shows a crack width over 5 times higher than the concrete. Clearly, the fibers of the ECC leads to a 100-fold reduction in the crack width compared to the ECC-Matrix although the total hygral deformation (100% to 0%) of both is the same.

The drying time when the first crack appears shows large differences. For the brittle ECC-matrix the one and only crack appeared after 1 day drying time. The quasi-brittle concrete took seven days of drying before the crack appeared. The first crack for the ductile ECC appeared after four days of drying. These cracks are hardly visible to the naked eyes. An optical microscope is necessary to measure the crack width.

CONCLUSIONS

The crack width of ECC under restrained drying shrinkage is a material property and is about 30-50μm (depending on cement type) at 50% RH for the mix compositions tested. This crack width is below the steady state crack width during strain-hardening and consistent with the crack width at strain value equal to the drying shrinkage strain (Fig. 4). In terms of durability the crack width is more important than the amount of free drying shrinkage, so that ECC should be more durable than concrete despite the higher free drying shrinkage. As a material property, the crack width of ECC is independent of structural dimension or reinforcement ratio.

ECC produced with a low alkali content (0.6M.-%) Portland cement leads to a 5% reduction in free drying shrinkage deformation and a 30% lower crack width at 50% RH compared to an ECC produced with a normal alkali content (0.9M.-%) Portland cement. It is desirable to produce ECC with LA-cement in order to improve the durability for RH < 50%. At RH > 50%, the influence of alkali content on free drying shrinkage and crack width of the ECCs investigated is negligible.

The hygral deformation of ECC can be explained by an expansion of CSH-gel particles due to a change of surface energy and by a repulsive disjoining pressure for RH > 40%. A reduction of disjoining pressure leads to lower drying shrinkage. Methods to reduce the disjoining pressure include the use of a LA-cement, the use of alkali free mixing water, and the addition of trivalent ions in the concrete composition or any combination of these.

The depth of penetration of water and aggressive agents due to capillary suction in a porous material is inversely proportional to the radius of cracks or pores which are assumed as capillary tubes. Treatment of the surface of ECC with a hydrophobic agent may be useful to further minimize penetration of water and aggressive agents into an ECC cover and protect the steel reinforcement from corrosion in reinforced ECC structures. Initial investigations into the use of hydrophobic agents in ECC were conducted by Martinola et al. [22].

ACKNOWLEDGEMENTS

Support by the NSF to the ACE-MRL and by the Deutsche Forschungsgemeinschaft (DFG) to M. Weimann to support his studies at the Univ. of Michigan are gratefully acknowledged.

REFERENCES

[1] Lide D.R.: *"Handbook of Chemistry and Physics"*, 77th, CRC Press, (2002)

[2] Li, V.C.: *"Engineered Cementitious Composites-Tailored Composites Through Micromechanical Modeling"*, in: Fiber Reinforced Concrete: Present and the Future, Eds. N. Banthia et al., CSCE, Montreal, pp. 64-97, (1998)

[3] Beltzung, F., Wittmann, F.H. and Holzer L.: *"Influence of Composition of Pore Solution on Drying Shrinkage"*, in: Creep, Shrinkage and Durability Mechanics of Concrete and other Quasi-Brittle Materials, Eds. Ulm, F.-J., Bazant, Z.P. and Wittmann, F.H., Elsevier Science Ltd., pp. 39-48, (2001)

[4] Derjaguin, B.V., Rabinovich, Y.I. and Churaev, N.V.: *"Direct Measurement of Molecular Forces"*, Nature, **272**, 5651, pp. 313-318, (1978)

[5] Adamson, A.W.: *"Physical Chemistry of Surfaces"*, John Wiley & Sons, Inc., (1997)

[6] Wittmann, F.H.: *"The Structure of Hardened Cement Paste - A Basis for a Better Understanding of the Materials Properties"*, in: Hydraulic Cement Paste: Their Structure and Properties, Cement and Concrete Ass., pp. 96-117, Slough, UK, (1976)

[7] Wittmann, F.H.: *"Creep and Shrinkage Mechanisms"*, in: Creep & Shrinkage in Concrete Structures, Eds. Bazant & Wittmann, Wiley & Sons, pp.129-161, (1982)

[8] Bangham, D. and Fakhoury, N.: *"The Translational Motion of Molecules in the Adsorbed Phase on Solids"*, J. Chemical Society, Part I, pp. 1324-1333, (1931)

[9] Hiller, K.H.: *"Strength Reduction and Length Changes in Porous Glass Caused by Water Vapor Adsorption"*, Journal of Applied Physics, **35**, 5, pp. 1622-1628, (1964)

[10] Yates, D.J.C.: *"Molecular Specificity in Physical Adsorption"*, Advances in Catalysis and Related Subjects, **12**, pp. 265-312, Academic Press Inc., (1960)

[11] Flood, E.A. and Heyding, R.D.: *"Stresses and Strains in Adsorbent-Adsorbate Systems"*, Canadian Journal of Chemistry, **32**, pp. 660-682, (1954)

[12] Wittmann, F.H.: *"Surface Tension, Shrinkage and Strength of Hardened Cement Paste"*, Materials and Structures, **1**, 6, pp. 547-552, (1968)

[13] Israelachvili, J. N.: *"Intermolecular and Surface Forces"*, Acad. Press Inc., (1992)

[14] Li, V.C., Wang, S. and Wu. C.: *"Tensile Strain-Hardening Behavior of Polyvinyl Alcohol Engineered Cementitious Composites (PVA-ECC)"*, **ACI** Materials Journal, pp. 483-492, (November-December 2001)

[15] **A**merican **S**ociety for **T**esting and **M**aterials (U.S. Code Organization)

[16] Greenspan, L.: *"Humidity Fixed Points of Binary Saturated Aqueous Solutions"*, J. Research of the NBS – Amer. Physics Chemistry, **81A**, 1, (January-February 1977)

[17] Schneider, A.: *"Diagramme zur Bestimmung der relativen Luftfeuchtigkeit"*, Holz als Roh- und Werkstoff (German Journal), 7, pp. 269-272, (1960)

[18] Shah, S.P., Karaguler, M.E. and Sarigaphuti, M.: *"Effect of Shrinkage-Reducing Admixtures on Restrained Shrinkage Cracking of Concrete"*, **ACI** Materials Journal, **89**, pp. 289-295, (May-June 1992)

[19] Wittmann, F.H.: *"Structure and Fracture Mechanics of Composite Materials"*, in: Fracture Toughness and Fracture Energy, Eds. H. Mihashi, H. Takahashi and F.H. Wittmann, A.A. Balkema Publishers, pp. 3-12, (1989)

[20] Weimann, M.: *"Vergleichende Studie der hygrischen Eigenschaften ausgewaehlter Werkstoffe des Bauwesens"*, Building Materials Reports No. 14, Aedificatio Verlag GmbH, Freiburg, Germany, (2001)

[21] Wang, K., Jansen, D.C. and Shah, S.P.: *"Permeability Study of Cracked Concrete"*, Cement and Concrete Research, **27**, 3, pp. 381-393, (1997)

[22] Martinola, G., Baeuml, M. & Wittmann F.H.: *"Modified ECC Applied as an Effective Chloride Barrier"*, Proc., JCI Int'l Workshop on DFRCC, pp. 171-180, (2002)